Optical properties of Cr^{3+} and Nd^{3+} in singly- and doubly-doped barium-indium-gallium-based fluoride glass investigated by time-resolved laser spectroscopy

M. J. Elejalde, R. Balda, J. Fernández, and E. Macho
Departamento de Física Aplicada I, Escuela Técnica Superior de Ingenieros Industriales y de Telecomunicación, Universidad del País Vasco, Alameda Urquijo s/n 48013 Bilbao, Spain

J. L. Adam
Université de Rennes, Campus de Beaulieu, Laboratoire de Chimie Minérale D, Avenue du Général Leclerc, 35042 Rennes CEDEX, France
(Received 30 March 1992)

The optical properties of Cr^{3+}-, Nd^{3+}-, and Cr^{3+}:Nd^{3+}-doped fluoride glass ($30BaF_2$-$18InF_3$-$12GaF_3$-$20ZnF_2$-$10YF_3$-$6ThF_4$-$4ZrF_4$) have been investigated in the 4.2–300-K temperature range at several concentrations by using steady-state and time-resolved laser spectroscopy. The luminescence of trivalent chromium in singly-doped glass shows a strong thermal quenching and can be analyzed on the basis of two broad statistical site distributions. The luminescence quenching of the $^4F_{3/2} \rightarrow {}^4I_{11/2}$ laser transition of Nd^{3+} in singly-doped glass has been studied by investigating the thermal and concentration dependence of lifetimes. A T^3 dependence for the nonradiative Nd^{3+}-Nd^{3+} relaxation has been found in the 15–100-K temperature range at high Nd^{3+} concentrations, which is in agreement with a two-site nonresonant process. Cr^{3+}-to-Nd^{3+} radiative and nonradiative energy transfer in codoped glass has been demonstrated from the emission spectra and the decrease of Cr^{3+} fluorescence lifetimes. The comparison between the time-resolved emission spectra of Cr^{3+} singly-doped and codoped samples indicates a very rapid $Cr^{3+} \rightarrow Nd^{3+}$ energy-transfer process with a lower limit of 10^7 s^{-1}. The nonradiative $Cr^{3+} \rightarrow Nd^{3+}$ energy transfer is consistent with an electric-dipole–electric-dipole interaction mechanism. The transfer efficiency corrected for Nd^{3+}-Nd^{3+} self-quenching is in agreement with the measured Nd^{3+} luminescence transferred by Cr^{3+} donors.

I. INTRODUCTION

It is well known that luminescence of trivalent rare-earth ions doped in inorganic solids can be enhanced or quenched by the presence of other kinds of rare-earth or transition-metal ions.[1] The mechanism that governs the transfer and diffusion of electronic excitation between the paramagnetic ions has been extensively studied[2–8] because of its interest in research and development of laser materials.

Among laser host materials, heavy-metal fluoride glasses have received much attention since their discovery 17 years ago because of their large transparency and facility to dissolve rare-earth or transition-metal ions. The optical properties of these ions have been extensively investigated by many authors. A list of relevant papers can be found in Refs. 9 and 10. More recently, fluoride glasses based on barium, indium, and gallium fluorides have been investigated because the multiphonon edge is located further away (8 μm), and promising applications as optical fibers operating up to 5 μm should be expected. As far as quantum efficiency is concerned, these glasses show multiphonon emission rates lower than fluorozirconate glasses.[11]

A knowledge of the most important laser parameters requires a detailed spectroscopic study as a function of concentration and temperature, relating optical properties with chemical composition of the host glass. Neodymium doped glasses are by far the most widely investigated systems, and many of the observed luminescence features for Nd^{3+} ions are also applicable to other rare earths.[9] On the other hand, the Cr^{3+} ion is likely to continue playing a central role in the development of solid-state laser materials because of the broad $^4T_2 \rightarrow {}^4A_2$ emission band which predominates in a weak crystal field octahedral environment. This electronic transition is also responsible for the efficient sensitization of Nd^{3+} if energy transfer from Cr^{3+} to Nd^{3+} is more probable than radiative or nonradiative relaxation of the $^4T_2$ state. Efficient nonradiative energy transfer from Cr^{3+} to Nd^{3+} has been observed in various glasses.[12–16] One of the conditions for nonradiative energy transfer is the spectral overlap of donor emission and acceptor absorption.[3] This condition is well fulfilled in heavy-metal fluoride glasses, where the broad $^4T_2 \rightarrow {}^4A_2$, Cr^{3+} emission band between 700 and 1200 nm overlaps the Nd^{3+} absorption. In recent works,[17–20] some of the authors investigated the optical properties of Cr^{3+} ion in heavy-metal fluoride matrices studying the influence of the glass composition on their spectral and temperature behavior.

The aim of this work is to describe the main features of Cr^{3+} to Nd^{3+} energy transfer in the fluoride glass of composition $30BaF_2$-$18InF_3$-$12GaF_3$-$20ZnF_2$-$10YF_3$-$6ThF_4$-$4ZrF_4$ (BIGaZYTZr) using steady-state and time-resolved spectroscopy, and to determine the transfer and luminescence efficiencies as a function of donor and ac-

ceptor concentrations, and temperature. Before considering the transfer problem the optical properties of singly doped Cr^{3+} and Nd^{3+} glasses are also investigated.

II. EXPERIMENTAL TECHNIQUES

Fluoride glass samples doped with various concentrations of chromium and neodymium were prepared at the Mineral Chemistry Laboratory of the Rennes University (France).

Samples were obtained with the molar composition $30BaF_2$-$18InF_3$-$12GaF_3$-$20ZnF_2$-$(10-x-y)YF_3$-$6ThF_4$-$4ZrF_4$-$xCrF_3$-$yNdF_3$ (BIGaZYTZr:Cr^{3+}:Nd^{3+}). The experimental method for preparing these fluoride glasses has been well described in the literature.[21–23] The concentration of both dopants in mol% is given in Table I.

The sample temperature was varied between 4.2 and 300 K with a continuous flow cryostat. Conventional absorption spectra were performed with a CARY 5 spectrophotometer. The emission measurements were made using the 633-nm emission line of a 15-mW He-Ne laser and the 514-nm emission line of an argon laser as exciting light. The fluorescence was analyzed with a 0.22-m SPEX monochromator, and the signal was detected by a Hamamatsu R7102 extended ir photomultiplier and finally amplified by a standard lock-in technique. The system response was calibrated with a standard tungsten-halogen lamp to correct the emission spectra.

Lifetime measurements were performed with a tunable dye laser (1-ns pulse width). In order to describe the evolution of fluorescence, time-resolved spectroscopy has been used. The emission measurements were obtained by exciting the sample with a tunable dye laser and detecting the emission with a Hamamatsu R7102 photomultiplier. The spectra were processed by a EGG-PAR boxcar integrator.

III. EXPERIMENTAL RESULTS

A. BIGaZYTZr:Cr^{3+}

1. Absorption and emission spectra

The absorption and emission spectra in glasses are usually interpreted by the Tanabe-Sugano diagram for d^3 systems with octahedral coordination, at least as far as the energy levels are concerned. The use of this diagram is justified because the Cr^{3+} ions tend to surround themselves octahedrally, and it has been shown that this is also the case in glasses.[18,24–29]

TABLE I. Dopant concentrations in mol% for the BIGaZYTZr fluoride glass.

Sample number	Cr^{3+} (mol%)	Nd^{3+} (mol%)
1	0.2	0
2	0	0.1
3	0	1
4	0	2
5	0	5
6	0.05	1
7	0.5	1
8	0.2	1
9	0.2	2
10	0.2	5

Figure 1(a) shows the room temperature (RT) absorption spectrum of Cr^{3+}(0.2%) singly-doped BIGaZYTZr fluoride glass. The absorption spectrum is characterized by two spin-allowed broad bands, which can be identified as the vibronically broadened transitions $^4A_2 \rightarrow {}^4T_2$ centered around 655 nm and $^4A_2 \rightarrow {}^4T_1$ around 450 nm. The $^4A_2 \rightarrow {}^4T_2$ absorption band shows a fine structure due to the spin-forbidden $^4A_2 \rightarrow {}^2E$ and $^4A_2 \rightarrow {}^2T_1$ transitions. The assignment of this structure has been made following the Fano antiresonance interpretation.[30–32] The Cr^{3+} emission spectrum in this glass is characterized by a broad and structureless band, centered about 890 nm which corresponds to the $^4T_2 \rightarrow {}^4A_2$ transition. This emission shows a large Stokes shift ($\approx$4000 cm^{-1}) and strongly decreases with increasing temperature.

2. Emission lifetime results

The decay kinetics of the broad infrared emission of Cr^{3+} in BIGaZYTZr fluoride glass were studied as a

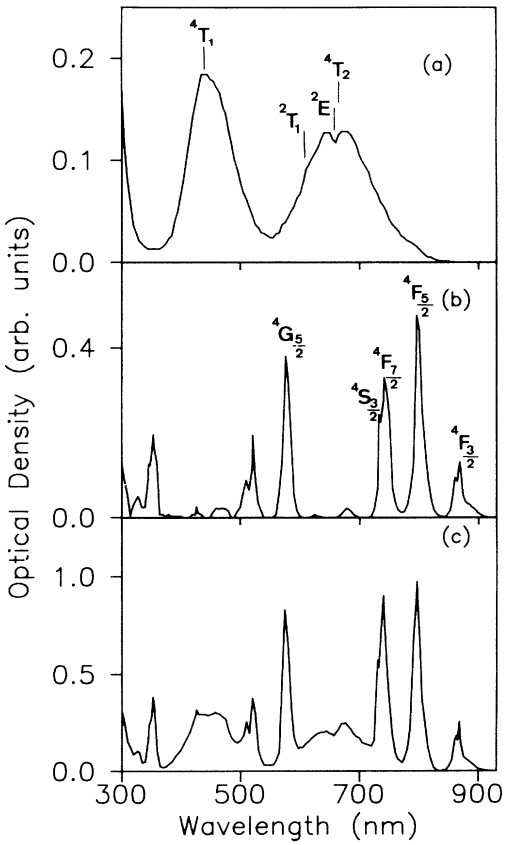

FIG. 1. Room-temperature absorption spectra of (a) Cr^{3+} (0.2%) singly-doped BIGaZYTZr fluoride glass, (b) Nd^{3+} (1%) singly-doped BIGaZYTZr fluoride glass, and (c) Cr^{3+} (0.2%):Nd^{3+} (1%) codoped fluoride glass.

function of temperature and emission wavelength. The observed decays measured along the broad emission band, under pulsed laser excitation, at the center of the $^4A_2 \rightarrow {}^4T_2$ absorption band (655 nm), can be described by a double-exponential function throughout the whole temperature range. This behavior persists even at lower concentrations ($\approx 0.05\%$), therefore indicating that chromium-chromium interactions are not to be considered important in this case. Figure 2 shows, as an example, the logarithmic plot of the intensity decay (excited at 655 nm) at liquid nitrogen temperature (LNT) for emission wavelengths of 820 and 1020 nm. These decays correspond to the singly-doped fluoride glass BIGaZYTZr:Cr^{3+} (0.2%) and are well described by the sum of two decaying exponentials. The short-lived and long-lived components of the experimental decays obtained by a least-squares fit are around 45 and 137 μs at LNT for an emission wavelength of 820 nm. These values are only a qualitative indication of the double-exponential character of the decays. It is evident from the figure, that the time dependence of the decays varies across the broad emission band shifting toward shorter decay times as the wavelength increases.

For practical purposes we shall use the "average lifetime" defined by equation $\bar{\tau} = \int tI(t)dt / \int I(t)dt$ in the analysis which follows. It is worthwhile noticing that the calculated $\bar{\tau}$ are very close to the lifetime values obtained by fitting the experimental curves to a singly-exponential function (deviations $|\bar{\tau} - \tau|$ are less than 10%), indicating the weak double-exponential character of the decays.

The spectral dependence of the decays along the broad emission band obtained under excitation at 655 nm is plotted in Fig. 3. As can be seen the lifetimes remain nearly constant on the high energy wing of the emission band but then decrease as energy decreases.

Lifetime data, monitored at 820 nm and integrated emission intensities $\int I(t)dt$ as a function of temperature, are shown in Fig. 4. The strong temperature dependence both of lifetimes and integrated emission intensities was most likely attributed to the dominance of multiphonon emission processes.[19]

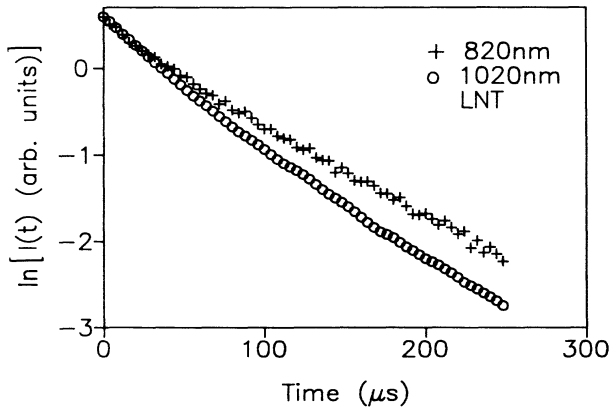

FIG. 2. Logarithmic plot of the decays of the $^4T_2 \rightarrow {}^4A_2$ transition in BIGaZYTZr:Cr^{3+} (0.2%) fluoride glass monitored at 820 and 1020 nm for an excitation wavelength of 655 nm. Measurements were performed at 77 K.

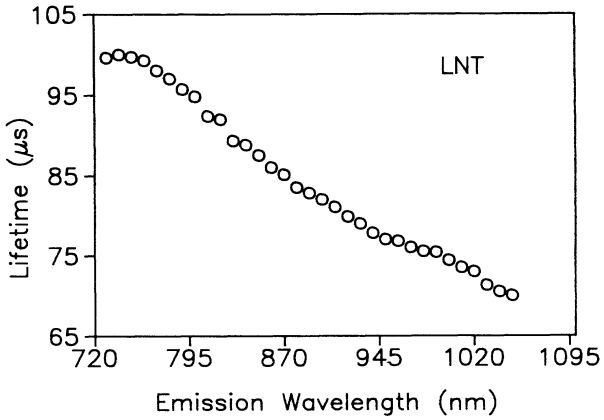

FIG. 3. LNT lifetimes at different emission wavelengths along the $^4T_2 \rightarrow {}^4A_2$ emission band of BIGaZYTZr:Cr^{3+} (0.2%) fluoride glass for an excitation wavelength of 655 nm. The data correspond to the average lifetime.

3. *Time-resolved emission spectra*

As we mentioned before, the absorption and emission spectra of Cr^{3+} doped glasses are consistent with the fact that Cr^{3+} lies in sites of nearly octahedral symmetry.[33] We might thus expect to have a large range of available sites for Cr^{3+} ions in glasses. In spite of this, there are experimental evidences, reported by some of the authors in heavy-metal and transition-metal fluoride glasses[18,29] pointing to the existence of two main site distributions of Cr^{3+} ions in these glasses.

In order to confirm this hypothesis also in the BIGaZYTZr fluoride glass matrix, time-resolved (TR) emission spectra were performed. These spectra were obtained at 77 K after exciting the sample with a tunable dye laser at the peak position of the $^4A_2 \rightarrow {}^4T_2$ absorption band. The evolution of the emission intensity at different time delays between 1 and 250 μs was investigated. At shorter time delays the spectrum shows similar features to the steady-state spectrum, but for increasing

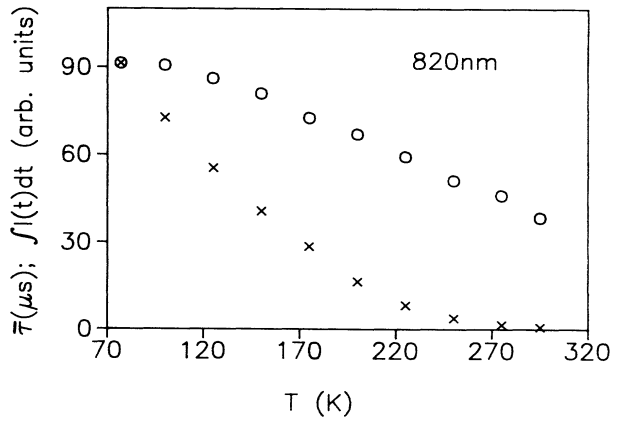

FIG. 4. Average lifetimes $\bar{\tau}$(○) and integrated emission intensities $\int I(t)dt$(×) as a function of temperature for BIGaZYTZr:Cr^{3+} (0.2%) fluoride glass.

time delays they show a blue shift and a narrowing of the bandwidth. Figure 5 displays the first and second moments, calculated from the TR emission spectra. As shown in this figure, the narrowing of the spectra and the peak shift do not exhibit a monotonic variation with increasing time as was observed in other systems.[34] In this case the variation is more pronounced at the first 50 μs, corresponding this time with the values for the short-lived component of the decays.

B. BIGaZYTZr:Nd^{3+}

1. Absorption and emission spectra

Similar experiments were performed on the BIGaZYTZr:Nd^{3+} system. The room-temperature absorption spectra of BIGaZYTZr:Nd^{3+} were measured in the 300–2500-nm spectral range. Figure 1(b) shows the absorption spectrum of Nd^{3+}(1%) sample in the 300–900-nm range of interest. The labels refer to the Russell-Saunders levels to which the ground-state ($^4I_{9/2}$) ions are excited. The absorption bands originating from the $^4I_{9/2}$ ground state were integrated, and these data, along with the values for the Nd^{3+} concentration and the refractive index were fitted by a computerized least-squares program to yield the best-fit values for the Judd[35]-Ofelt[36] (JO) parameters Ω_2, Ω_4, Ω_6. To estimate the JO parameters we have utilized the reduced matrix elements, $\|U^t\|^2$, reported by Carnall *et al.*[37] for Nd^{3+} ions in LaF_3. The obtained values ($\Omega_2=1.31\times10^{-20}$, $\Omega_4=2.71\times10^{-20}$, $\Omega_6=4.01\times10^{-20}$ cm^2) are in good agreement with those previously referenced for the Nd^{3+} ion in different glass materials.[11,38–43]

The quality of the fit obtained from the absorption spectrum of Nd^{3+} in this glass is shown in Table II, where f_m is the measured absorption line strength obtained from the absorption spectrum integration and f_c is the calculated absorption line strength obtained by using the expression proposed in Judd's theory.[35]

The various radiative parameters for each emission level of the Nd^{3+} ions in this glass can be calculated using the Ω_t parameters determined from the least-squares fitting of absorption data. In Table III we report the results for the radiative transition probabilities (A), the branching ratios (β_R), and the total spontaneous emission probability (W_R), calculated for the laser emission state $^4F_{3/2}$. The calculated value for the radiative lifetime was 537 μs. According to Jacobs and Weber,[38] the intensity of the $^4F_{3/2}\rightarrow{}^4I_{11/2}$ laser transition is dependent only on the Ω_4 and Ω_6 parameters. For a large cross section Ω_4 and Ω_6 are required to be as large as possible. Since Ω_2 does not enter the branching ratios for the Nd^{3+}, $^4F_{3/2}$ fluorescence can be expressed in terms of the

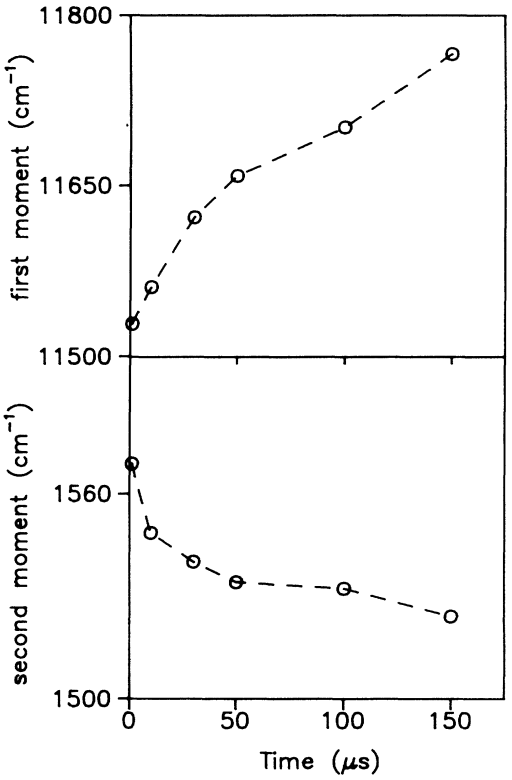

FIG. 5. Time dependence of first and second moments obtained from the corrected time-resolved emission spectra of BIGaZYTZr:Cr^{3+} (0.2%) fluoride glass. The time-resolved emission spectra were obtained at 77 K by exciting at 655 nm with time delays between 1 and 250 μs and gate widths between 50 ns and 1 μs. The broken curves are only a guide for the eye.

TABLE II. Measured (f_m) and calculated (f_c) absorption line strengths for Nd^{3+} in BIGaZYTZr:Nd^{3+} (1%) fluoride glass.

Transition	λ (nm)	$10^{-8}f_m$	$10^{-8}f_c$	$10^{-8}(f_m-f_c)$
$^4I_{9/2}\rightarrow{}^4I_{13/2}$	2502.0	110.70	108.31	2.39
$^4I_{15/2}$	1649.0	22.82	16.01	6.81
$^4F_{3/2}$	869.4	136.63	141.04	−4.41
$^4F_{5/2}$, $^2H_{9/2}$	797.9	508.06	501.27	6.79
$^4F_{7/2}$, $^4S_{3/2}$	740.9	516.53	545.02	−28.49
$^4F_{9/2}$	679.3	36.83	40.51	−3.68
$^2H_{11/2}$	627.4	9.59	11.38	−1.79
$^4G_{5/2}$, $^2G_{7/2}$	577.1	775.83	783.27	−7.44
$^2K_{13/2}$, $^4G_{7/2}$, $^4G_{9/2}$	516.9	436.31	346.299	90.02
$^2K_{15/2}$, $^2G_{9/2}$, $^2D_{3/2}$, $^4G_{11/2}$	466.7	116.73	84.92	31.81
$^2P_{1/2}$, $^2D_{5/2}$	427.1	32.51	39.17	−6.66

TABLE III. Radiative property parameters for the $^4F_{3/2} \rightarrow {}^4I_J$ ($J=9/2$, 11/2, 13/2, 15/2) transitions of BIGaZYTZr:Nd^{3+} (1%) fluoride glass.

Transition	$A(J,J')$ (s^{-1})	β_R
$^4F_{3/2} \rightarrow {}^4I_{15/2}$	9.9	0.005
$^4F_{3/2} \rightarrow {}^4I_{13/2}$	195.4	0.105
$^4F_{3/2} \rightarrow {}^4I_{11/2}$	950.6	0.511
$^4F_{3/2} \rightarrow {}^4I_{9/2}$	704.0	0.379
W_R (s^{-1})	1859.9	

Ω_4/Ω_6 ratio. To maximize the fluorescence intensity to $^4I_{11/2}$ one wants $\Omega_4 \ll \Omega_6$. From the values of Ω_4 and Ω_6 obtained for BIGaZYTZr: Nd^{3+}(1%) fluoride glass, the spectroscopic quality factor $\Omega_4/\Omega_6=0.68$ is in agreement with the large β_R value for the $^4F_{3/2} \rightarrow {}^4I_{11/2}$ transition.

The $^4F_{3/2} \rightarrow {}^4I_{11/2}$ steady-state emission spectrum at 1058 nm was measured at different temperatures by exciting the samples with the 514-nm line of an argon laser. The effective fluorescence linewidth corresponding to the room-temperature (RT) spectra for all Nd^{3+} concentrations are reported in Table IV. This effective fluorescence linewidth was determined by integrating the fluorescence line shape and dividing by the intensity at the peak fluorescence emission wavelength.[38] The radiative transition probability for emission together with the recorded luminescence spectra makes it possible to evaluate the stimulated emission cross section of $^4F_{3/2} \rightarrow {}^4I_{11/2}$ for the four samples. These values were obtained using Eq. (8) in Ref. 44, and are also displayed in Table IV.

Time-resolved emission spectra for this transition were also performed by exciting the samples with a tunable dye laser at the $^4I_{9/2} \rightarrow {}^4G_{5/2}$ absorption band (575 nm) at different time delays after laser pumping. No significant variations were observed for the emission peak position and bandwidth, as time increases between 1 and 700 μs. This behavior can be expected because in heavy-metal fluoride glasses, rare-earth ions are embedded in well-defined sites of the glass-forming network.[45]

2. Emission lifetime results

The decays of the $^4F_{3/2} \rightarrow {}^4I_{11/2}$ transition for four Nd^{3+} concentrations (0.1, 1, 2, and 5%) were obtained under laser excitation at the $^4I_{9/2} \rightarrow {}^4G_{5/2}$ absorption band (575 nm) as a function of temperature. These decays were found to be the single exponential for all temperatures and concentrations. The lifetimes values as a function of temperature between 4.2 and 300 K are presented in Fig. 6.

The radiative lifetime, calculated from the absorption parameters and measured fluorescence lifetimes of the four samples at RT are given in Table IV. The ratio of these lifetimes yields the calculated radiative quantum efficiency presented in the same table.

C. BIGaZYTZr:Cr^{3+}:Nd^{3+} fluoride glass

1. Absorption and emission spectra

The room-temperature absorption spectrum of codoped BIGaZYTZr fluoride glass, for Cr^{3+} and Nd^{3+} concentrations of 0.2% and 1%, respectively, is shown in Fig. 1(c). The spectrum shows the typical broad absorption bands of Cr^{3+} in addition to the narrow Nd^{3+} transitions.

Figure 7 shows the steady-state emission spectra of the same sample obtained at different temperatures (4.2, 77, and 295 K) by exciting at 633 nm into the $^4A_2 \rightarrow {}^4T_2$ absorption band. At this wavelength only Cr^{3+} absorbs, so the appearance of the Nd^{3+} fluorescence around 890 nm ($^4F_{3/2} \rightarrow {}^4I_{9/2}$) and the $^4F_{3/2} \rightarrow {}^4I_{11/2}$ emission at 1058 nm shows that energy transfer from Cr^{3+} to Nd^{3+} occurs. The dips around 790 and 870 nm, observed in the emission spectra, are due to Nd^{3+} absorption. There is excitation of Nd^{3+} by direct absorption of photons emitted by Cr^{3+}, indicating the existence of radiative energy transfer. As can be seen from this figure the total emission intensity substantially decreases with increasing temperature.

2. Emission lifetime results

Characteristic decays of the codoped glass were obtained under laser pulsed excitation at the center of the $^4A_2 \rightarrow {}^4T_2$ absorption band (655 nm) as a function of temperature at different emission wavelengths for all samples. The lifetimes for Cr^{3+} were measured at 820 nm and the Nd^{3+} emission was followed by monitoring the 1058-nm emission line. The 820-nm emission originated from the $^4T_2$ level of Cr^{3+} exhibited a nonexponential behavior with an average lifetime of about 41 μs. The same behavior was found for the three samples with a different Cr^{3+} concentration. The shortening of the lifetime (≈ 50 μs) as compared with the singly-doped sample, is ascribed to nonradiative energy transfer to Nd^{3+}. When the Nd^{3+} concentration increases, the Cr^{3+} decays become faster indicating an increasing transfer rate. Figure 8 gives the logarithmic plot of the intensity decays at 77 K moni-

TABLE IV. Room temperature emission properties of Nd^{3+} singly-doped BIGaZYTZr fluoride glass.

	$^4F_{3/2} \rightarrow {}^4I_{11/2}$				
	τ_R (μs)	τ_{expt} (μs)	η_Q	$\Delta\nu_{eff}$ (cm^{-1})	σ_p (10^{20} cm^2)
Nd (0.1%)		447	0.83	232	2.68
Nd (1%)	537	409	0.76	229	2.68
Nd (2%)		317	0.59	224	2.66
Nd (5%)		95	0.18	231	2.68

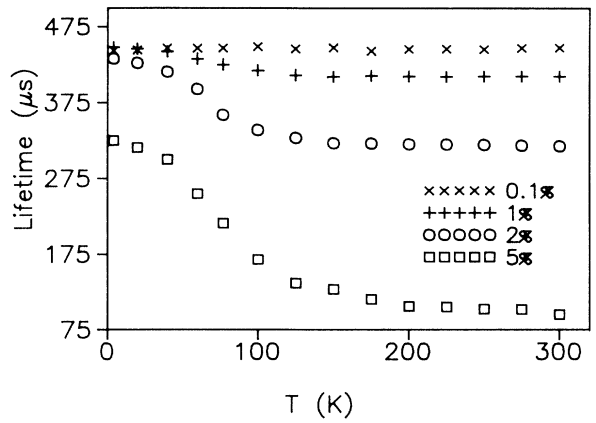

FIG. 6. Lifetimes as a function of temperature for singly-doped Nd^{3+} glass with different Nd^{3+} concentrations. (×) 0.1%, (+) 1%, (○) 2%, and (□) 5%. Lifetimes were obtained by exciting at 575 nm and collecting the fluorescence at the emission peak of the ${}^4F_{3/2} \rightarrow {}^4I_{11/2}$ transition.

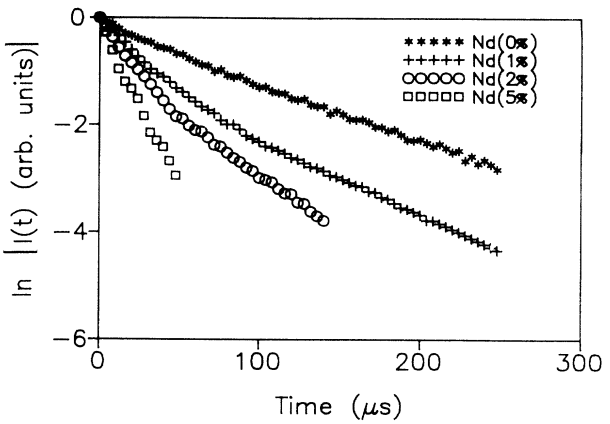

FIG. 8. Logarithmic plot of the fluorescence decays of the ${}^4T_2 \rightarrow {}^4A_2$ emission monitored at 820 nm, in the codoped BIGaZYTZr fluoride glass with Cr^{3+} (0.2%) and different Nd^{3+} concentrations, zero included, for an excitation wavelength of 655 nm. Measurements correspond to 77 K.

tored at 820 nm for a 0.2% Cr^{3+} concentration and different Nd^{3+} concentrations, zero included. Figure 9 presents the LNT logarithmic plot of the 1058-nm emission for the codoped glass with three different Nd^{3+} concentrations. The decay is exponential in all cases and the lifetime decreases as the Nd^{3+} concentration increases.

The fluorescence decays for the 820- and 1058-nm emissions were also measured as a function of temperature. The decay time of the Cr^{3+} emission was measured in all samples in the 77–295-K range. The values of these lifetimes are shown in Fig. 10, which also includes, for comparison, the lifetime of BIGaZYTZr:Cr^{3+}(0.2%) singly-doped fluoride glass already reported in Fig. 4. The data correspond to the "average lifetime." Because of the intensity decrease of Cr^{3+} emission when Nd^{3+} concentration increases, there was some difficulty in the accurate measurements of lifetimes for the sample with a 5% of Nd^{3+} above 100 K.

The decays obtained at the 1058-nm Nd^{3+} emission by exciting the Cr^{3+} ions into the ${}^4A_2 \rightarrow {}^4T_2$ absorption band (655 nm) are presented in Fig. 11. As can be seen from this figure the lifetimes decrease as Nd^{3+} concentration increases, and are temperature dependent.

3. *Time-resolved emission spectra*

The time-resolved emission spectra of Cr^{3+} singly-doped and Cr^{3+},Nd^{3+}-codoped fluoride glasses were taken at liquid nitrogen temperature at different time delays after pulsing. Figure 12 presents the TR emission spectra for the sample with 0.2% of Cr^{3+} and 1% of Nd^{3+} at different time delays ranging from 100 ns to 200 μs (gate widths ranging from 10 ns to 1 μs). The spectra are vertically shifted for better visualization and are scaled to have a similar height. These spectra show, superimposed to the Cr^{3+} emission, the Nd^{3+} emission around 890 and

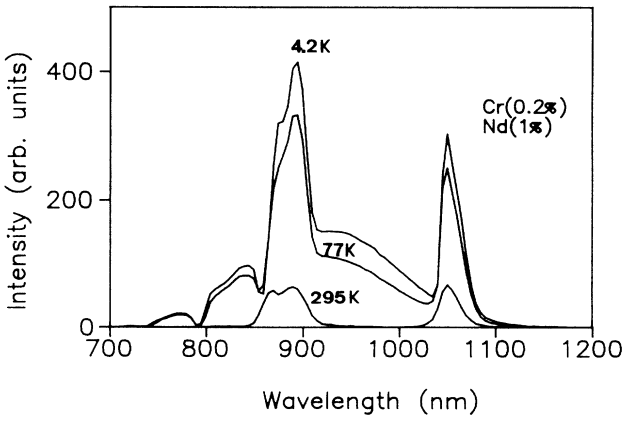

FIG. 7. Steady-state (SS) emission spectra of BIGaZYTZr:Cr^{3+} (0.2%):Nd^{3+} (1%) fluoride glass, obtained at different temperatures (4.2, 77, and 295 K) by exciting at the ${}^4A_2 \rightarrow {}^4T_2$ absorption band with the 633-nm line of a He-Ne laser. The spectra are not corrected for the spectral response of the system.

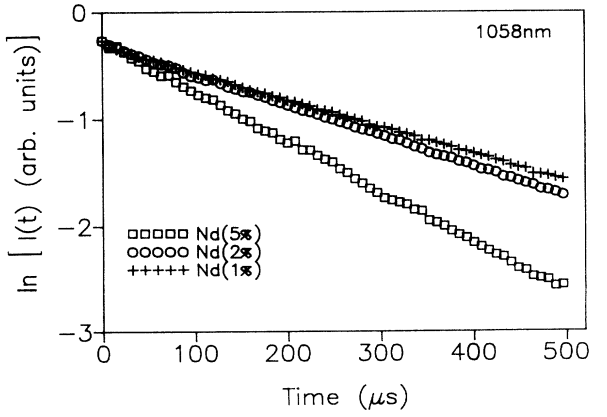

FIG. 9. Logarithmic plot of the fluorescence decays of the ${}^4F_{3/2} \rightarrow {}^4I_{11/2}$ emission monitored at 1058 nm, in the codoped BIGaZYTZr fluoride glass with Cr^{3+} (0.2%) and different Nd^{3+} concentrations: (+) 1%, (○) 2%, and (□) 5%, for an excitation wavelength of 655 nm. Measurements correspond to 77 K.

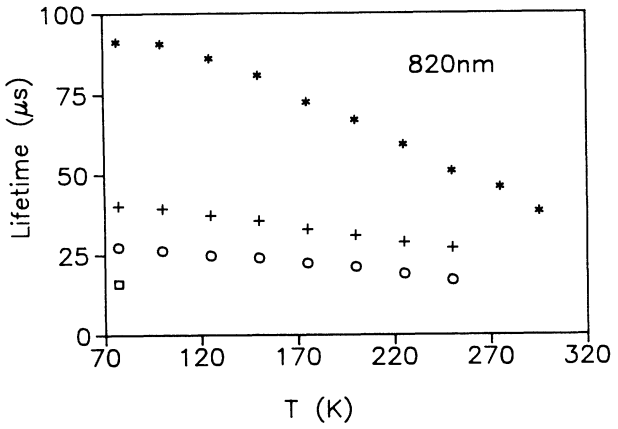

FIG. 10. Lifetimes of the Cr^{3+} emission as a function of temperature in BIGaZYTZr:Cr^{3+} (0.2%) singly-doped fluoride glass (*) and in the codoped samples: (+) Cr^{3+} (0.2%):Nd^{3+} (1%), (○) Cr^{3+} (0.2%):Nd^{3+} (2%), and (□) Cr^{3+} (0.2%):Nd^{3+} (5%). Lifetimes were obtained by exciting at the center of the $^4A_2 \rightarrow {}^4T_2$ absorption band (655 nm) and collecting the fluorescence at 820 nm.

1058 nm, and two dips around 790 and 870 nm due to radiative absorption by Nd^{3+} absorption bands in this spectral range. These results show that even at quite a short time, radiative and nonradiative energy transfer to Nd^{3+} exists. As can be seen from this figure, there is a decrease in the emission of the $^4T_2$ level of Cr^{3+} as time delay increases from 100 ns to 200 μs. The emission decay of Cr^{3+} ($\approx$41 μs) is much faster than the decay of the $^4F_{3/2}$ ($\approx$400 μs) of Nd^{3+}, and therefore at 200 μs after pulsing, the $^4T_2$ emission of Cr^{3+} nearly disappears, while emission originating from $^4F_{3/2}$ level still exists. This behavior was found to be independent of Cr^{3+} concentration.

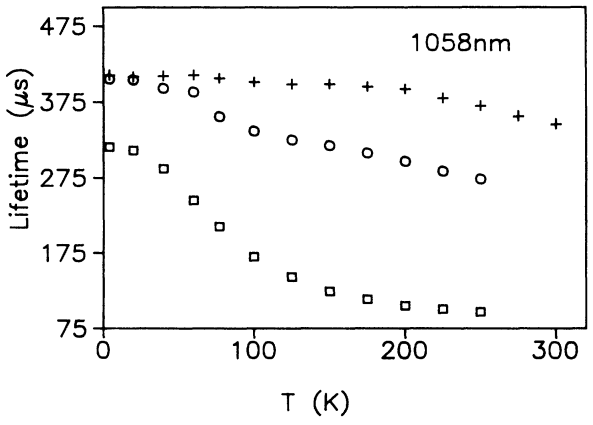

FIG. 11. Lifetimes as a function of temperature for all codoped samples with Cr^{3+} (0.2%). Lifetimes were obtained by exciting at the center of the $^4A_2 \rightarrow {}^4T_2$ absorption band (655 nm) and collecting at the emission peak of the $^4F_{3/2} \rightarrow {}^4I_{11/2}$ transition. (+) Nd^{3+} (1%), (○) Nd^{3+} (2%), and (□) Nd^{3+} (5%).

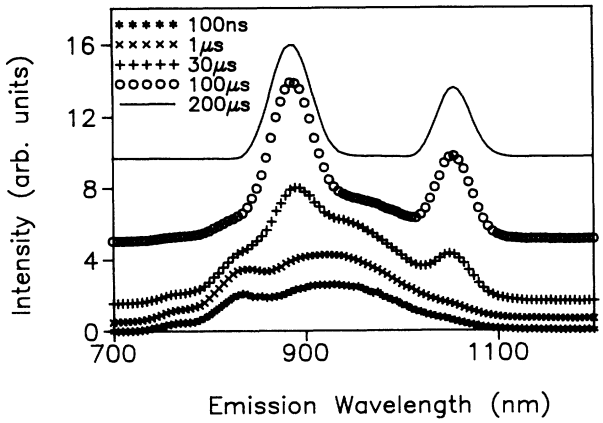

FIG. 12. Time-resolved emission spectra taken at different time delays (between 100 ns and 200 μs) for the codoped fluoride glass BIGaZYTZr:Cr^{3+} (0.2%):Nd^{3+} (1%). The spectra are scaled and vertically shifted for better visualization. Measurements were performed at 77 K, for an excitation wavelength of 655 nm.

IV. DISCUSSION

A. BIGaZYTZr:Cr^{3+}

As we mentioned before, the main features of the absorption and emission spectra of Cr^{3+} in BIGaZYTZr fluoride glass can be broadly interpreted in terms of a crystal-field diagram. Because of the structural disorder inherent to a glass we might expect a large continuous range of slightly distorted octahedral sites available to Cr^{3+} ions. Nevertheless, the experimental results on fluorescence lifetimes and time-resolved spectra, shown in Sec. III A, point to the existence of two main site distributions for Cr^{3+} ions in BIGaZYTZr fluoride glass. Figure 3 (Sec. III A) showed the average lifetimes within the $^4T_2 \rightarrow {}^4A_2$ emission band after excitation with the 655-nm line. It is worthwhile noticing that at short wavelengths the lifetime remains nearly constant and then decreases linearly as the wavelength increases throughout the $^4T_2 \rightarrow {}^4A_2$ emission band. If a homogeneous site distribution were to be present, a monotonic decrease of lifetimes with increasing emission wavelength should be expected. These results are consistent with a model of two or more subsets of Cr^{3+} ions with a slightly different spectral dependence. The double-exponential character shown by the shape of lifetime curves under laser excitation also reinforces this hypothesis. As we shall see below, energy transfer or cross relaxation between Cr^{3+} in spectrally different sites can be disregarded as shown by time-resolved fluorescence.

The influence of different sites on the time dependence of emission spectra may help to clarify our understanding of Cr^{3+} site distributions. At short time delays (1 μs) the TR emission spectra do not show significant differences from the SS spectra, and the fluorescence is characteristic of the whole distribution of ions. When time increases, the ions with the shorter lifetimes have decayed and make no contribution to the delayed fluorescence. As a consequence a blueshift and a monotonic narrowing

should appear.[34] In spite of this, Fig. 5 showed that the blueshift and half-width narrowing display an abrupt change in the time interval between 1 and 50 μs which roughly covers the short-lived component of the experimental decays. If energy transfer or cross relaxation between Cr^{3+} ions were present, energy would migrate toward the lower energy sites giving a redshift instead of the blueshift observed.

The Cr^{3+} emission in this glass shows a strong temperature dependence (see Fig. 4) attributed to an increase of nonradiative transitions. The thermal quenching of the luminescence for Cr^{3+} in a similar matrix of composition $30BaF_2$-$18InF_3$-$12GaF_3$-$20ZnF_2$-$10YF_3$-$10ThF_4$ (BIGaZYT) has been reported by some of the authors.[19] In this study the thermal quenching was discussed in terms of the quantum-mechanical single configurational-coordinate QMSCC model[46] with different constant forces in the ground and excited states, and a quite good agreement with the experimental results was found. We have compared the temperature dependence of nonradiative decay rates for Cr^{3+} in BIGaZYT[19] and BIGaZYTZr fluoride glasses and no significant difference was found, therefore confirming the same thermal quenching mechanism.

B. $Nd^{3+} \rightarrow Nd^{3+}$ energy transfer

The lifetime of $^4F_{3/2}$ state of Nd^{3+} ion in the singly-doped glass should be governed by a sum of probabilities for several competing processes: radiative decay, nonradiative decay by multiphonon emission, and by energy transfer to other Nd^{3+} ions. At low temperatures and low concentrations, the measured lifetimes are singly exponential and nearly approach to the predicted purely radiative rate, hence the rate of nonradiative decay by multiphonon emission must be small. As the concentration rises the decay remains singly exponential but a decrease in the experimental lifetime is observed (see Fig. 6) even at helium temperature. This behavior could be associated with rapid energy diffusion between Nd^{3+} ions that can lead to a spatial equilibrium within the Nd^{3+} system. In the transfer rapid limit the donor transfer takes place so quickly that the transfer times for different donor-acceptor pairs are averaged out and the whole system exhibits a simple exponential decay as is experimentally observed.[47,48]

This behavior was also found in another Nd^{3+} doped system by carrying out measurements at different concentrations and temperatures.[49,50] In our case the measured lifetime of the $^4F_{3/2}$ state at 4.2 K for the 0.1% Nd^{3+} sample is about 16% lower than the calculated radiative lifetime using the Fuchtbauer-Ladenburg equation.[44] This discrepancy seems too high to be related to the JO model and we think it is probably due to the onset of fast transfer processes between Nd^{3+} ions. Figure 13 shows the decay rates (τ^{-1}) of 0.1, 1, 2, and 5 % Nd^{3+} samples at room, liquid nitrogen, and liquid helium temperatures. An outstanding result is that the decay rates are nearly linear dependent on concentration at low temperatures. This result has also been found by other authors in concentrated Nd^{3+} systems and the implications of fast

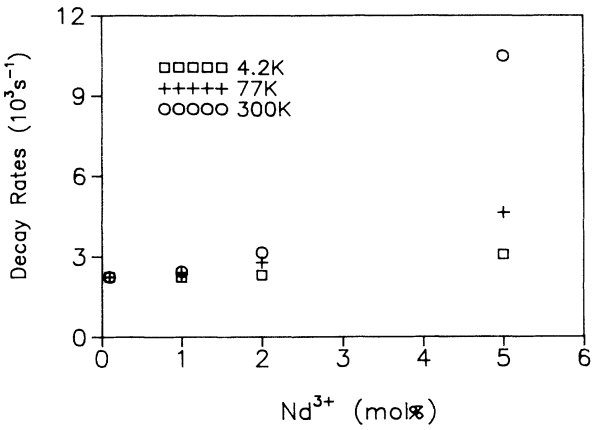

FIG. 13. Decay rates (τ^{-1}) of singly-doped BIGaZYTZr:Nd^{3+} fluoride glass as a function of concentration at different temperatures: (□) 4.2 K, (+) 77 K, and (○) 300 K.

diffusion on the concentration dependence of Nd^{3+} self-quenching have been pointed out.[49,50]

A detailed study of the thermal dependence of lifetimes was presented in Fig. 6. These results suggest the presence of a quite strong thermal quenching mechanism between 15 and 100 K. As mentioned above the multiphonon relaxation rate for the $^4F_{3/2}$ manifold is expected to be small because of the high energy gap to the next lower-lying J manifold (5438 cm^{-1}) and the typical values of phonon energies involved ($\approx$450 cm^{-1}). If we disregard these multiphonon relaxation processes, relaxation via fast Nd-Nd diffusion processes and subsequent deexcitation via energy sinks should be taken into account, as they occur even at low temperatures. In order to evaluate the temperature dependence of these nonradiative Nd-Nd relaxation processes we have used the experimental measured lifetimes and the simple relation

$$\tau_{\text{expt}}^{-1} = \tau_R^{-1} + W_{\text{Nd-Nd}}(T) ,$$

where τ_{expt} is the measured lifetime and τ_R represents the radiative lifetime. Figure 14 shows the plot of $[W_{\text{Nd-Nd}}(T) - W_{\text{Nd-Nd}}(0)]^{1/3}$ in the 15–100-K range for 2% and 5% Nd^{3+} concentrations. It is worthwhile noticing the good fitting of $W_{\text{Nd-Nd}}$ to a T^3 dependence. This could correspond to a two-site nonresonant process in the short-wavelength regime as has been shown by Holstein *et al.*[51] In this process, the phonon emission and absorption takes place at different sites, the ion-phonon interaction acts twice, and the site-site Hamiltonian once. This phonon-assisted excitation transfer between different states of similar ions could be understood by taking into account a small spread in the energy values of $^4F_{3/2}$ transitions to the J multiplicity due to the inherent disorder of the glass structure. Under these conditions two phonon processes can dominate whether (i) the two-phonon-assisted transfer coherence factor shows lack of interference or (and) (ii) because of a small phonon density of states at the energy mismatch.[51]

Due to the singly-exponential character of lifetimes for all concentrations and temperatures no attempt was made to investigate any other possible physical process

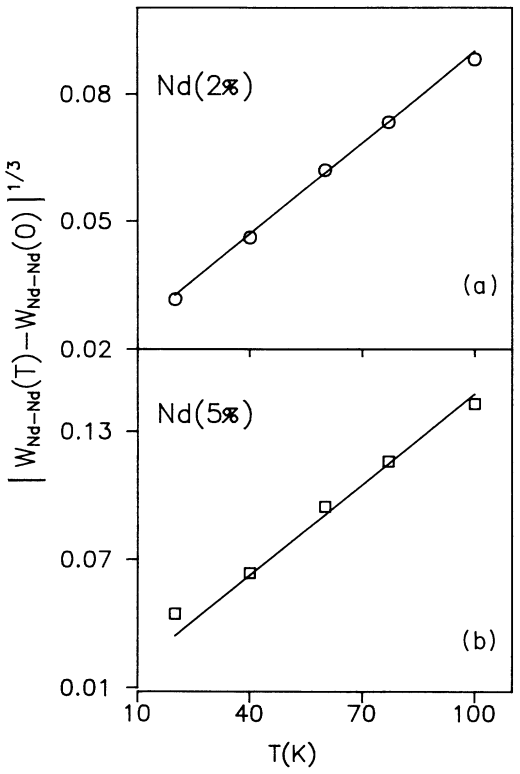

FIG. 14. Plot of the nonradiative Nd-Nd relaxation rate in the 15–100-K temperature range for (a) BIGaZYTZr:Nd^{3+} (2%) and (b) BIGaZYTZr:Nd^{3+} (5%) fluoride glasses. Symbols stand for the experimental values, and solid lines are the fit to a T^3 dependence.

for the Nd-Nd interaction leading to the observed luminescence thermal quenching.

C. $Cr^{3+} \rightarrow Nd^{3+}$ energy transfer

As we have seen in Sec. III C pulsed selective excitation and steady-state measurements of codoped Cr^{3+}, Nd^{3+} BIGaZYTZr fluoride glass have demonstrated the existence of efficient Cr^{3+} to Nd^{3+} energy transfer. It was also evident that together with a nonradiative transfer a radiative contribution exists as shown by the dips in the emission spectra (see Fig. 7). In order to evaluate this contribution and establish time-scale limits for the energy transfer, very careful time-resolved emission spectra were performed at 100-ns, 500-ns, and 1-μs time delays, exciting the Cr^{3+} ions in three codoped samples (Cr^{3+} 0.2%, Nd^{3+} 1, 2, and 5%). Since only the qualitative comparison between emission spectra was of interest, no corrections were made for the spectral response of the system. Figures 15–17 show these spectra normalized with the one obtained for the Cr^{3+} (0.2%) singly-doped fluoride glass at the same time delays. As can be seen from these figures the substraction curve between the scaled TR emission spectra of Cr^{3+} (0.2%) singly-doped fluoride glass and the TR emission of codoped samples with Cr^{3+} (0.2%), Nd^{3+} (1, 2, and 5%) shows the two Nd^{3+} emissions at 890 and 1058 nm and the Nd^{3+} absorptions corresponding to the dips observed around 790 and 870 nm. From these results, some conclusions can be inferred. (i) The radiative contribution to the transfer represented by the dips around 790 and 870 nm shows a weak dependence on Nd^{3+} concentration and amounts to a 10% of the whole Cr^{3+} emission for the sample with 1% Nd^{3+}. No appreciable changes are observed for different time delays. (ii) As time and Nd^{3+} concentration increase, the luminescence from the $^4F_{3/2} \rightarrow {}^4I_{11/2}$, $I_{9/2}$ is enhanced and can be easily identified at the upper side of the base line showing that an effective transfer occurs. (iii) $Cr^{3+} \rightarrow Nd^{3+}$ transfer is already present below 100 ns, corresponding to transfer rates higher than $10^7\ s^{-1}$ which are faster than the nonradiative relaxation of Cr^{3+} in the singly-doped fluoride glass ($\approx 10^4\ s^{-1}$).

The presence of nonradiative $Cr^{3+} \rightarrow Nd^{3+}$ energy transfer was demonstrated by observing the time-dependent behavior of the Cr^{3+} fluorescence from the codoped samples. As has been shown in Fig. 8 the Cr^{3+} decay becomes faster when Nd^{3+} concentration increases

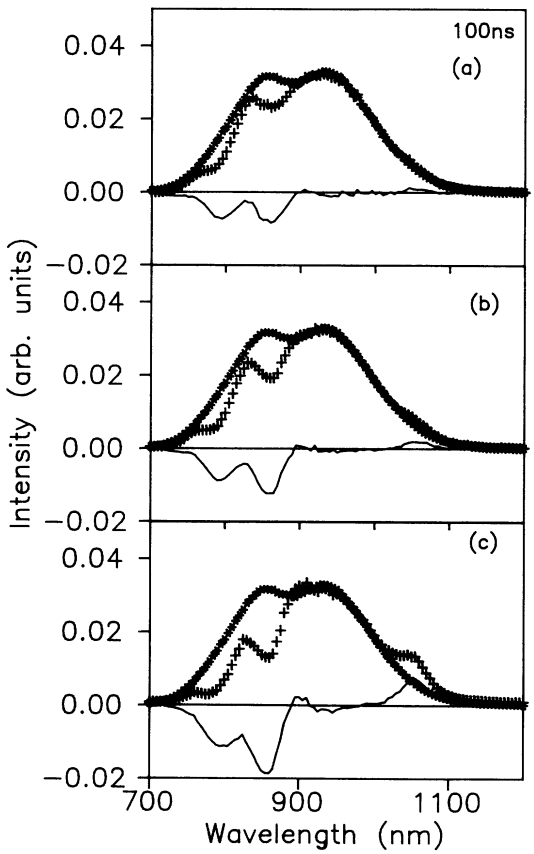

FIG. 15. Comparison between (×) time-resolved emission spectrum of $^4T_2 \rightarrow {}^4A_2$ transition in BIGaZYTZr:Cr^{3+} (0.2%) fluoride glass at a time delay of 100 ns, and (+) time-resolved emission spectrum of the codoped glass obtained at the same time delay. The scaled difference between both spectra is represented by a solid line. (a) BIGaZYTZr:Cr^{3+} (0.2%):Nd^{3+} (1%), (b) BIGaZYTZr:Cr^{3+} (0.2%):Nd^{3+} (2%), and (c) BIGaZYTZr:Cr^{3+} (0.2%):Nd^{3+} (5%) fluoride glasses. The spectra were obtained by exciting at 655 nm. Measurements were performed at 77 K.

because of the additional nonradiative relaxation probability. On the other hand, the Cr^{3+} emission from the $^4T_2$ level of a singly-chromium-doped BIGaZYTZr fluoride glass (also shown in Fig. 2), shows an intrinsic double-exponential behavior, which can be related with the existence of slightly different statistical distributions of Cr^{3+} ion environments. As energy transfer can be excluded between donors (see Sec. IV A) only direct energy transfer to acceptors can affect the Cr^{3+} lifetime at a given temperature. The transfer can occur via multipolar or exchange interactions,[3] with the electric dipole-dipole transfer process as the most probable one at the concentrations used.[52] According to the Inokuti-Hirayama model,[4] if higher-order processes can be neglected, the normalized donor decay curves can be expressed by

$$\Phi(t)=\exp\left[-\frac{t}{\tau_0}-\frac{4}{3}\pi\Gamma\left[1-\frac{3}{s}\right]N_i R_0^3\left[\frac{t}{\tau_0}\right]^{3/s}\right], \tag{1}$$

with $S=6$, 8, and 10, respectively, for electric dipole-dipole, dipole-quadrupole, and quadrupole-quadrupole interactions. N_i is the acceptor concentration and R_0 is the critical transfer distance defined as the distance for which the probability for energy transfer between a given donor-acceptor pair is equal to the donor intrinsic decay probability τ_0^{-1}. Although it is difficult to establish the exact multipolar nature of the $Cr^{3+}\rightarrow Nd^{3+}$ transfer process we have found that a dipole-dipole transfer is consistent with the experimental decay intensities if account is taken of the short and long-lived components of the Cr^{3+} intrinsic lifetimes. Figure 18(a) shows a least-square fit of the experimental Cr^{3+} decay at LNT of a Cr^{3+}(0.2%),Nd^{3+}(1%)-codoped BIGaZYTZr fluoride glass sample to Eq. (1) using the Cr^{3+} intrinsic average lifetime τ_0. The obtained value for R_0 was 9 ± 1 Å. Figure 18(b) gives the fitting to the linear combination $\lambda_1\Phi(t,\tau_0^l)+\lambda_2\Phi(t,\tau_0^s)$ based on Eq. (1) using the values of τ_0 belonging to the short (s) and long-lived (l) components of the intrinsic Cr^{3+} decays.

Using the Dexter[3] energy transfer probability $W(r_{ij})$ for interionic dipole-dipole coupling and the above definition of R_0, it is possible to obtain an independent way of evaluating R_0 (and therefore of testing the dipole-dipole hypothesis):

$$W(r_{ij})=\frac{3h^4c^4Q_j}{64\pi^5 r_{ij}^6 n^4\tau_i}K\int\frac{F_i(E)F_j(E)}{E^4}dE\ , \tag{2}$$

where Q_j is the absorption cross section of the acceptor ion j, r_{ij} is the separation of the donor-acceptor pair, τ_i the donor radiative lifetime, and K is a local field correction factor (which can be taken ≈1).[52] In the spectral overlap integral $F_i(E)$ and $F_j(E)$ are normalized line-

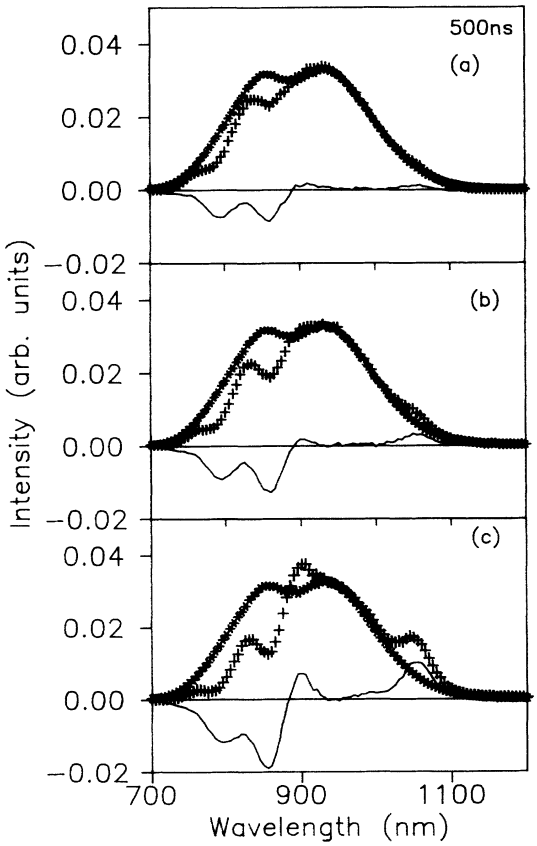

FIG. 16. The same comparison as in Fig. 15 but at a time delay of 500 ns.

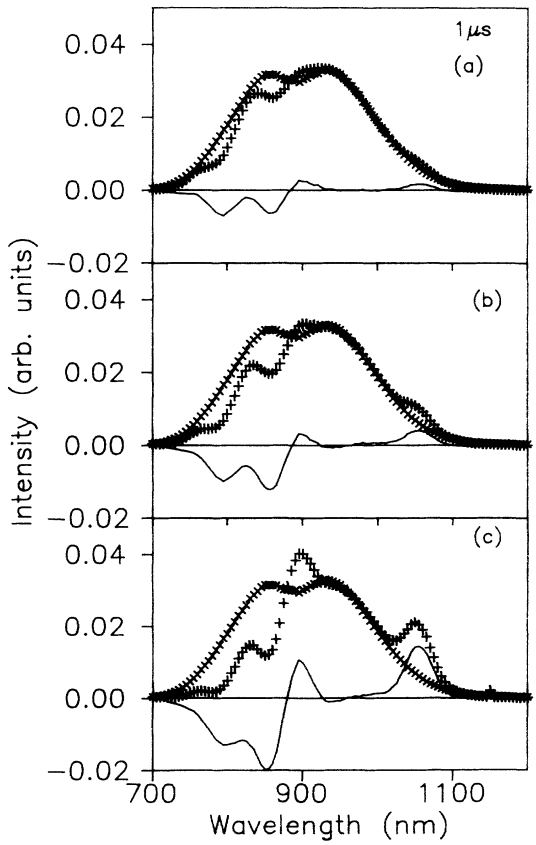

FIG. 17. The same comparison as in Figs. 15 and 16 but at a time delay of 1 μs.

shape functions for the donor emission and acceptor absorption, respectively. Taking $r_{ij}=R_0$ in Eq. (2), then $W\tau_i=1$, and R_0 can be found from the relation[3,53]

$$R_0^6=\eta\frac{3h^4c^4Q_j}{64\pi^5n^4}\int\frac{F_i(E)F_j(E)}{E^4}dE\ , \tag{3}$$

where η is the quantum efficiency of the Cr^{3+} emission. Using data from the spectra of the Cr^{3+}(0.2%),Nd^{3+}(1%)-codoped sample a value of $R_0=10\pm1$ Å is obtained. Account taken of the inherent errors in the preceding calculations, this value supports the dipole-dipole coupling hypothesis. An average critical distance R_0 was also estimated at room temperature for the three codoped samples using the relation[50] $\tilde{R}=(3/4\pi C)^{1/3}$, where C is the Nd^{3+} acceptor concentration. The results were $\tilde{R}$(Å)=10.3, 8.2, and 6.0 for the 1%, 2%, and 5% Nd^{3+} concentration, respectively. The value of 10.3 Å for the 1% Nd^{3+} sample is well in accordance with the above calculations.

1. *Transfer efficiency*

The transfer efficiency was estimated according to the expression

$$\eta_t(\tau)=1-\frac{\tau}{\tau_0}\ , \tag{4}$$

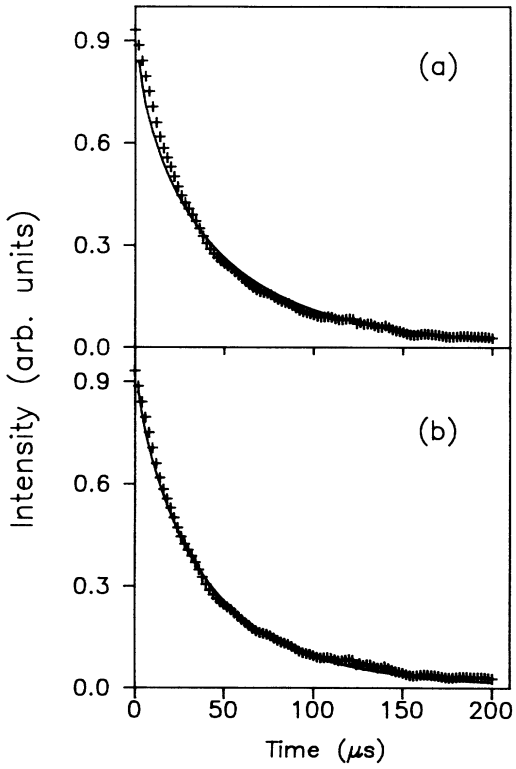

FIG. 18. Cr^{3+} emission showing the fitting between the experimental decay curves (+) and the calculated ones (solid lines) for BIGaZYTZr:Cr^{3+} (0.2%):Nd^{3+} (1%) fluoride glass: (a) using the average lifetime of Cr^{3+} at 820 nm and (b) using the short-lived and long-lived components of the Cr^{3+} decay. Measurements correspond to 77 K.

with τ and τ_0 being the Cr^{3+} mean-decay times monitored at 820 nm, with and without Nd^{3+} ions. Figure 19 gives the Cr^{3+} to Nd^{3+} transfer efficiency and the estimated quantum efficiency of the Nd^{3+} emission as a function of Nd^{3+} concentration for a 0.2% Cr^{3+} sample at 77 K. (No appreciable dependence on transfer efficiency was observed on Cr^{3+} concentration.) As can be seen, the transfer is quite efficient at high Nd^{3+} concentrations. However, because of the strong luminescence quenching of Nd^{3+} with concentration (see Sec. IV B) it is obvious that a compromise should be reached for maximizing the luminescence emitted by Nd^{3+} as a consequence of transfer. In order to clarify this point, Nd^{3+} luminescence emission measurements were performed on the codoped samples in such a way that an absolute comparison could be made among different Nd^{3+} concentrations. The following procedure was used.[54] The fluorescence of the three codoped samples was excited using the 633-nm line of a power established He-Ne laser. The samples were thin slabs cut and polished to have exactly the same thickness. The pumping radiation was focused into the sample using a microscope stage with a 0.25-m monochromator and a photomultiplier at the tube end. A low magnifying objective was used for a close approximation to the upper surface of the sample. To avoid the direct entrance of the pumping light on the monochromator appropriate filters were used. Moreover, the Bertrand lens of the polarizing microscope could be also used to slightly misalign the path of the remaining pumping light reaching the entrance slit of the monochromator. The sample was placed so that the spectrometer collected all the luminescence coming from the sample volume contained within the solid angle subtended by the microscope objective. The recorded fluorescence of the measured samples normalized to the 2% Nd^{3+} sample is given in Fig. 20. As can be observed this sample has the highest luminescence efficiency. In the same figure we also show the theoretical efficiency $\eta=\eta_t\eta_Q$ calculated by using the values of the transfer efficiency η_t and the quantum efficiency η_Q of the Nd^{3+} emission. It

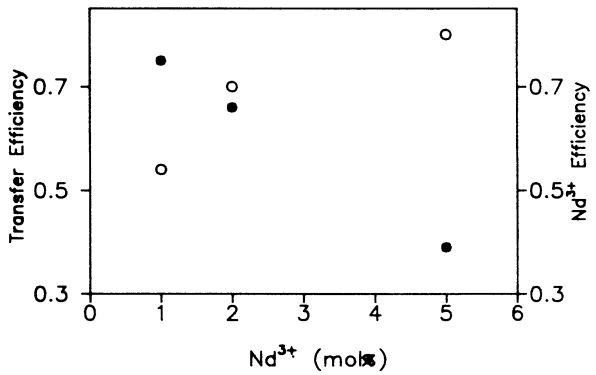

FIG. 19. $Cr^{3+}\rightarrow Nd^{3+}$ transfer efficiency calculated for an emission wavelength of 820 nm (○), and Nd^{3+} estimated quantum efficiency (●) vs Nd^{3+} concentration in the codoped samples with a Cr^{3+} concentration of 0.2%. Data correspond to 77 K.

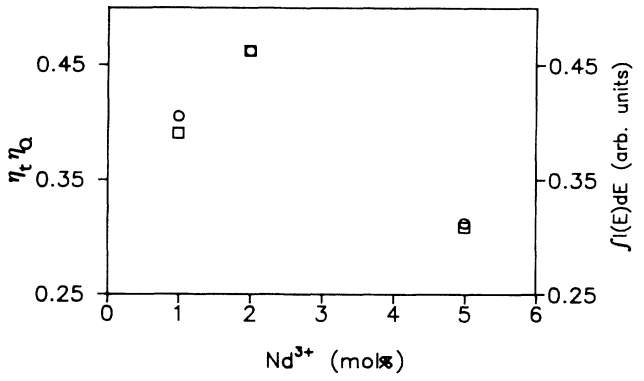

FIG. 20. Integrated emission intensities of the $^4F_{3/2}\rightarrow{}^4I_{11/2}$ transition (□), and theoretical efficiency $\eta=\eta_t\eta_Q$(○), calculated by using the values of the transfer efficiency η_t and the quantum efficiency η_Q of the Nd^{3+} emission, as a function of Nd^{3+} concentration for the three codoped samples with a Cr^{3+} concentration of 0.2%.

is worthwhile noticing the good agreement obtained by the two different approaches.

Figure 21 shows the transfer efficiencies for the different samples as a function of temperature. Because of the aforementioned difficulties for measuring lifetimes in the 5% Nd^{3+} codoped fluoride glass, only the value at 77 K is shown for this concentration. Finally, in Fig. 22 a comparison between luminescence thermal quenching of the Nd^{3+} emission from level $^4F_{3/2}$ for singly-doped and codoped fluoride glasses is shown. The decrease of lifetimes with temperature is somewhat different for the lowest Nd^{3+} concentration. In fact, a small nonexponential portion was observed at the initial part of the decay in the 1% Nd^{3+} codoped fluoride glass at 4.2 K, pointing to a weak $Nd^{3+}\rightarrow Cr^{3+}$ back transfer process. Figure 23 shows the logarithmic plots of the 1% Nd^{3+} singly-doped and codoped samples. As can be observed the long-term components of the decays are the same. At higher temperatures, the nonexponential part of the decay disappears. For higher Nd^{3+} concentrations only single-

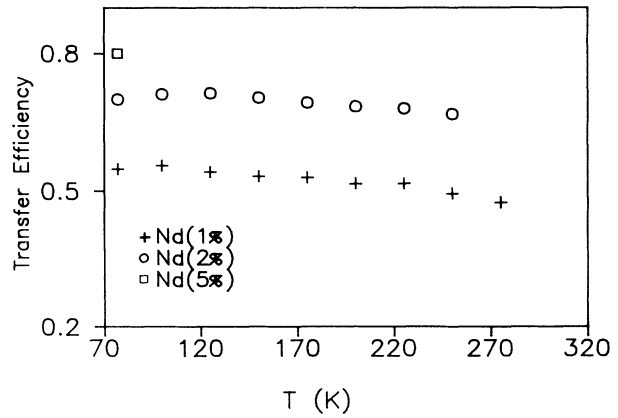

FIG. 21. Transfer efficiency as a function of temperature calculated for an emission wavelength of 820 nm, in codoped BIGaZYTZr:Cr^{3+}:Nd^{3+} fluoride glass samples with Cr^{3+} (0.2%).

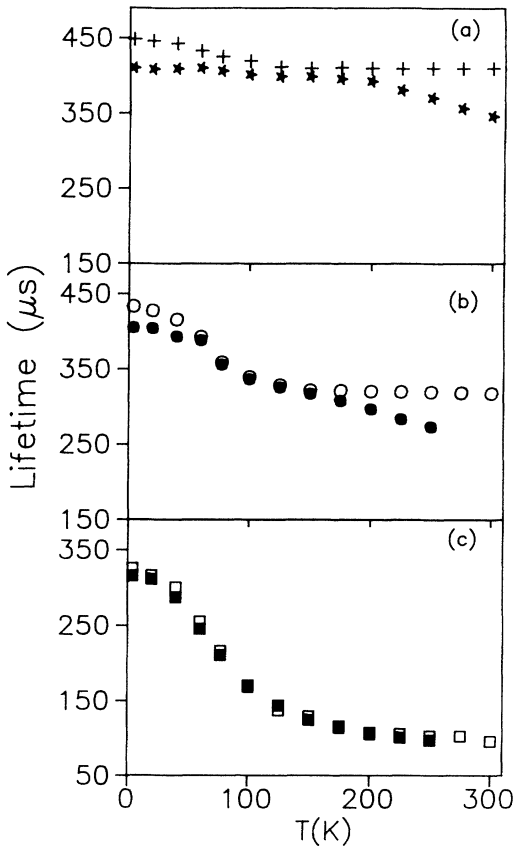

FIG. 22. Lifetime data as a function of temperature for Nd^{3+} singly-doped fluoride glass (obtained by exciting at 575 nm) and the codoped sample with the same Nd^{3+} concentration (obtained by exciting at 655 nm), monitored at 1058 nm. (a) (+) Nd^{3+} (1%), (★) Cr^{3+} (0.2%):Nd^{3+} (1%), (b) (○) Nd^{3+} (2%), (●) Cr^{3+} (0.2%):Nd^{3+} (2%), and (c) (□) Nd^{3+} (5%), (■) Cr^{3+} (0.2%):Nd^{3+} (5%).

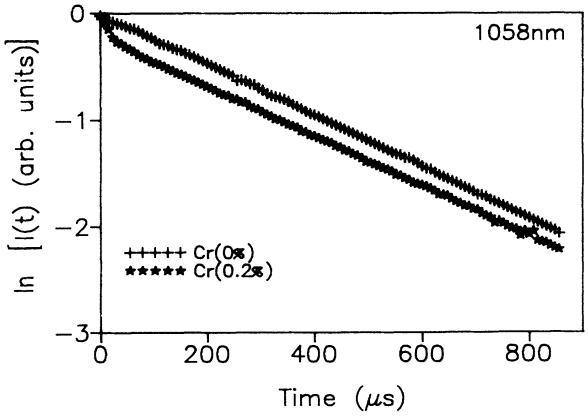

FIG. 23. Logarithmic plot of the fluorescence decays of the $^4F_{3/2}\rightarrow{}^4I_{11/2}$ emission monitored at 1058 nm, in the codoped BIGaZYTZr fluoride glass with Cr^{3+} (0.2%), Nd^{3+} (1%) (obtained by exciting at 655 nm) and in the singly-doped BIGaZYTZr:Nd^{3+} (1%) fluoride glass (obtained by exciting at 575 nm). Measurements correspond to 4.2 K.

exponential decays are observed, revealing that Nd-Nd fast diffusion dominates over any other deexcitation process.

V. CONCLUSIONS

From the above results the following conclusions can be reached.

(i) From the steady-state optical absorption and luminescence measurements we conclude that Cr^{3+} is incorporated, on the average, in octahedrally coordinated sites. The blueshift and narrowing of time-resolved emission spectra, together with the wavelength dependence shown by lifetimes along the $^4T_2 \rightarrow {}^4A_2$ emission band, and the double-exponential character of the decay can be related with the existence of two slightly different statistical distributions of Cr^{3+} ion environments.

(ii) The emission lifetimes from the $^4F_{3/2}$ state in the Nd^{3+} singly-doped samples are single exponential. As the concentration rises the decay remains single exponential but a decrease in the experimental lifetime is observed even at helium temperatures, indicating that relaxation via fast Nd-Nd diffusion processes occurs. The luminescence thermal quenching of $^4F_{3/2} \rightarrow {}^4I_{11/2}$ transition has been investigated from the thermal behavior of lifetimes and a T^3 dependence for the nonradiative Nd-Nd relaxation processes has been found in the 15–100-K temperature range at Nd^{3+} concentrations higher than 1% which is in agreement with a two-site nonresonant process.

(iii) Cr^{3+} to Nd^{3+} radiative and nonradiative energy transfer has been demonstrated from the emission spectra and the decrease of the Cr^{3+} fluorescence lifetime. The comparison between time-resolved emission spectra from Cr^{3+} singly-doped and codoped samples allows us to qualitatively evaluate the contribution of radiative energy transfer which shows a weak dependence on Nd^{3+} concentration and time.

(iv) Although it is difficult to establish the exact multipolar nature of the $Cr^{3+} \rightarrow Nd^{3+}$ transfer process, dipole-dipole transfer is consistent with the experimental decay intensities if account is taken of the short- and long-lived components of the Cr^{3+} intrinsic lifetime.

(v) The characteristic critical transfer distance R_0 is determined for the BIGaZYTZr:Cr^{3+}(0.2%),Nd^{3+}(1%) fluoride glass sample from two different sources, the decay curves of Cr^{3+} in the presence of Nd^{3+}, and the spectral data for Cr^{3+} and Nd^{3+} ions. The obtained values (≈ 10 Å) show a good agreement supporting the dipole-dipole transfer hypothesis.

(vi) Transfer efficiency, which has been studied as a function of donor and acceptor concentration, and temperature, reaches an 80% for the highest Nd^{3+} concentration. No appreciable dependence was observed on Cr^{3+} concentration.

(vii) Nd^{3+} luminescence emission measurements in the codoped samples have been performed in such a way that an absolute comparison could be made among different Nd^{3+} concentrations. The codoped sample with a 2% of Nd^{3+} shows the best luminescence efficiency in agreement with the highest theoretical efficiency calculated by using the values of the $Cr^{3+} \rightarrow Nd^{3+}$ transfer efficiency and the quantum efficiency of the Nd^{3+} emission.

ACKNOWLEDGMENTS

This work was supported by the Comisión Interministerial de Ciencia y Tecnología (CICYT) of the Spanish Government (Ref. No. 0188/89), Basque Country Government (Ref. No. PGV 9012), Ministerio de Educación y Ciencia (Acción Integrada Hispano-Francesa 9A y 18B), and Basque Country University (Ref. No. E126/91).

[1]E. Nakazawa and S. Shionoya, J. Chem. Phys. **47**, 3211 (1967).
[2]T. Förster, Ann. Phys. (Leipzig) [Folge 6] **2**, 55 (1948).
[3]D. L. Dexter, J. Chem. Phys. **21**, 836 (1953).
[4]M. Inokuti and F. Hirayama, J. Chem. Phys. **43**, 1978 (1965).
[5]Th. P. J. Botden, Phillips Res. Rep. **7**, 197 (1952).
[6]D. L. Dexter and H. H. Schulman, J. Chem. Phys. **22**, 1063 (1954).
[7]M. Yokota and O. Tanimoto, J. Phys. Soc. Jpn. **22**, 779 (1967).
[8]M. J. Weber, Phys. Rev. B **4**, 2932 (1971).
[9]M. J. Weber, J. Non-Cryst. Solids **123**, 208 (1990).
[10]J. Lucas and J. L. Adam, Glastech. Ber. **62**, 422 (1989).
[11]J. L. Adam, N. Rigout, E. Dénoue, F. Smektala, and J. Lucas, Proc. SPIE **1581** (1991).
[12]R. Reisfeld, in *Energy Transfer Processes in Condensed Matter,* edited by B. Di Bartolo (Plenum, New York, 1984), p. 521.
[13]J. G. Edwards and S. Gomulka, J. Phys. D. **12**, 187 (1979).
[14]A. G. Avasenov *et al.* Kvant. Electron. (Moscow) **6**, 1583 (1979) [Sov. J. Quantum Electron. **9**, 935 (1979)].
[15]T. Härig, G. Huber, and I. A. Shcherbakov, J. Appl. Phys. **52**, 4450 (1981).
[16]A. Van Die, A. J. Faber, G. Blasse, and W. F. Van Der Weg, J. Phys. Chem. Solids **47**, 1081 (1986).
[17]R. Balda, M. A. Illarramendi, J. Fernández, and J. Lucas, J. Lumin. **45**, 87 (1990).
[18]R. Balda, J. Fernández, M. A. Illarramendi, M. A. Arriandiaga, J. L. Adam, and J. Lucas, Phys. Rev. B **44**, 4759 (1991).
[19]M. A. Illarramendi, J. Fernández, R. Balda, J. Lucas, and J. L. Adam, J. Lumin. **47**, 207 (1991).
[20]J. Fernández, M. A. Illarramendi, R. Balda, M. A. Arriandiaga, J. L. Adam, and J. Lucas, J. Non-Cryst. Solids **131-133**, 1230 (1991).
[21]M. G. Drexhage, in *Treatise on Materials Science and Technology,* edited by M. Tomozawa and R. H. Doremus (Academic, New York, 1985), Vol. 26, pp. 151–243.
[22]A. Lecoq and M. Poulain, Verres Réfract. **34**, 333 (1980).
[23]J. Lucas, I. Chiaruttini, G. Fonteneau, P. Christensen, and S. Mitachi, Proc. SPIE **1228** (1990).
[24]L. J. Andrews, A. Lempicki, and B. C. McCollum, J. Chem. Phys. **74**, 5526 (1981).
[25]G. O. Karapetyan, S. G. Lunter, and D. M. Yudin, Opt. Spectrosc. **14**, 370 (1963).
[26]H. L. Schlafer, H. Gausmann, and H. Witzke, J. Chem. Phys. **46**, 1423 (1967).
[27]R. E. Tischer, J. Chem. Phys. **48**, 4291 (1968).
[28]A. van Die, G. Blasse, and W. F. van der Weg, Mat. Chem. Phys. **14**, 513 (1986).

[29]R. Balda, J. Fernández, M. J. Elejalde, M. A. Illarramendi, and C. Jacoboni, J. Phys.: Condens. Matter **3**, 7695 (1991).
[30]J. Fano, Phys. Rev. **124**, 1866 (1961).
[31]A. Lempicki, L. J. Andrews, S. Nettle, B. C. McCollum, and E. I. Solomon, Phys. Rev. Lett. **44**, 1234 (1980).
[32]M. A. Illarramendi, J. Fernández, and R. Balda, J. Lumin (to be published).
[33]G. F. Imbusch, T. J. Glynn, and G. P. Morgan, J. Lumin. **45**, 63 (1990).
[34]M. J. Weber, S. A. Brawer, and A. J. DeGroot, Phys. Rev. B **23**, 11 (1981).
[35]B. R. Judd, Phys. Rev. **127**, 750 (1962).
[36]G. S. Ofelt, J. Chem. Phys. **377**, 511 (1962).
[37]W. T. Carnall, P. R. Fields, and K. Rajnak, J. Chem. Phys. **49**, 4424 (1968).
[38]R. R. Jacobs and M. J. Weber, IEEE J. Quantum Electron. **QE12**, 102 (1976).
[39]R. Reisfeld and C. K. Jørgensen, *Lasers and Excited States of Rare Earths* (Springer-Verlag, Berlin, 1977), p. 111.
[40]C. Brecher, L. A. Riseberg, and M. J. Weber, Phys. Rev. B **18**, 5799 (1978).
[41]M. J. Weber, in *Laser Spectroscopy of Solids,* Topics in Applied Physics Vol. 49, edited by W. M. Yen and P. M. Selzer (Springer, Berlin, 1981).
[42]G. F. Neilson and M. C. Weinberg, J. Non-Cryst. Solids **28**, 209 (1978).
[43]J. Lucas, M. Chanthanasinh, M. Poulain, M. Poulain, P. Brun, and M. J. Weber, J. Non-Cryst. Solids **27**, 273 (1978).
[44]W. F. Krupke, IEEE J. Quantum Electron. **QE10**, 450 (1974).
[45]J. L. Adam, V. Ponçon, J. Lucas, and G. Boulon, J. Non-Cryst. Solids **91**, 191 (1987).
[46]C. W. Struck and W. H. Fonger, J. Lumin. **10**, 1 (1975).
[47]D. L. Huber, in *Laser Spectroscopy of Solids* (Ref. 41), p. 38.
[48]M. J. Weber, Phys. Rev. **4**, 2932 (1971).
[49]Y. K. Voronko *et al.*, Zh. Eksp. Teor. Fiz. **71**, 478 (1976) [Sov. Phys. JETP **44**, 251 (1976)].
[50]W. Lenth, G. Huber, and D. Fay, Phys. Rev. B **23**, 3877 (1981).
[51]T. Holstein, S. K. Lyo, and M. Orbach, in *Laser Spectroscopy of Solids* (Ref. 41), p. 83.
[52]R. R. Jacobs, C. B. Layne, and M. J. Weber, J. Appl. Phys. **47**, 2020 (1976).
[53]B. Di Bartolo, *Optical Interactions in Solids* (Wiley, New York, 1968).
[54]The procedure is based to a certain extent on the one developed by S. Shing, R. G. Smith, and L. G. van Uitert, Phys. Rev. B **10**, 2566 (1974).